Journal of
Mechanics of
Materials and Structures

AN ESHELBY-TYPE APPROACH FOR DEFECT ENERGETICS IN CARBON NANOTUBES

Liang Zhang and Jia Lu

Volume 2, № 2 February 2007

mathematical sciences publishers

JOURNAL OF MECHANICS OF MATERIALS AND STRUCTURES
Vol. 2, No. 2, 2007

AN ESHELBY-TYPE APPROACH FOR DEFECT ENERGETICS IN CARBON NANOTUBES

LIANG ZHANG AND JIA LU

This paper presents a method for characterizing the formation energy of Stone–Wales defect transformation in deforming carbon nanotubes. A formula is derived to show that the structural energy variation consists of the change of atomic potential due to bond reconfiguration in a local defective region, and an elastic correction that represents the influence of the remaining system. The advantage of the method lies in its computational efficiency. Specifically, global optimization for the configuration of the defective tube is eliminated. We use the method to investigate the formation energy distribution in nonuniformly deforming nanotubes, and to study the energetic interaction between multiple defects. Accuracy of the method is also assessed through numerical experiments.

1. Introduction

When loaded beyond a certain limit, carbon nanotubes (CNTs) respond to mechanical load via the formation of topological defects [Buongiorno Nardelli et al. 1998a; 1998b]. In a stretched CNT, a fundamental defect appears via a 90° rotation of a C-C bond from the predominantly transverse direction to the predominantly axial direction. This transition, known as the Stone–Wales (SW) transformation [1986], preserves the threefold sp^2 bond structure but replaces the hexagon rings with two pentagon-heptagon (5-7-7-5) pairs as indicated in Figure 1. At large stretches the bond rotation releases the excessive strain [Buongiorno Nardelli et al. 1998a; 1998b] and results in an energetically favorable state. The SW defect is active at high temperatures, and further relaxation through successive rotations at neighboring bonds becomes energetically favorable [Samsonidze et al. 2002a]. In this case, the SW transition furnishes a mechanism of "intramolecular plasticity" [Yakobson 1998; Buongiorno Nardelli et al. 1998a; 1998b]. At low temperatures, SW defects are not as active but their presence weakens the local stiffness [Chandra et al. 2004] and presents a potential site for crack nucleation. Recent studies reported that a SW defect can significantly reduce the limit strain of a carbon nanotube [Zhang et al. 1998; Zhang and Crespi 2000; Zhao et al. 2002; Troya et al. 2003; Mielke et al. 2004], and also affect the electrical properties of CNTs [Choi et al. 2000; Liu et al. 2004b; Nordlund and Hakonen 2005].

The formation energy, namely the energy difference between the defective and the maiden states, is a significant factor in defect kinetics. For a transformation to be energetically favorable, the defective state should rest at a lower energy level. Hence, a negative formation energy is often taken as the necessary condition for defect formation. In order to trigger the transformation, however, the system must receive sufficient energy to overcome the activation energy barrier [Samsonidze et al. 2002b; Buongiorno Nardelli et al. 1998a; Zhao et al. 2002]. It has been reported that a SW defect in a tensile CNT

Keywords: Stone–Wales defect, carbon nanotube, Eshelby method.
This work was partially supported by a Scientific Research Initiative Grant from the University of Iowa.

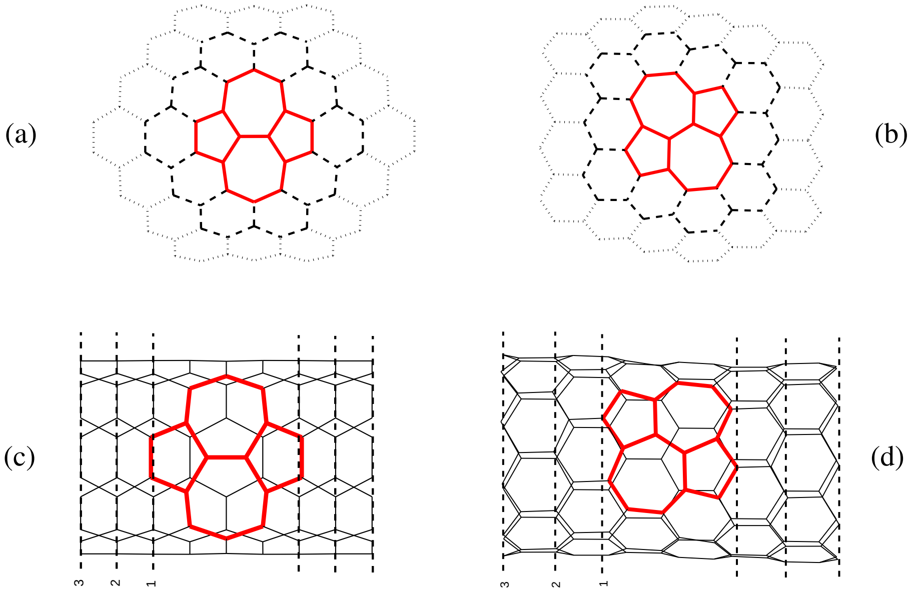

Figure 1. Illustration of the defective patches: (a) and (b) are layer models for large diameter tubes; (c) and (d) are ring models for small diameter tubes.

becomes energetically favorable at about 5–6% strain. However, at lower temperatures the activation barrier for this formation remains high and thus hinders the defect creation [Zhao et al. 2002]. The formation energy nevertheless remains an important indicator as it reflects the tendency of defect formation and the thermodynamical stability of the defect. In [Samsonidze et al. 2002a], for example, the energy of multiple SW defects as a function of the relative position is used to evaluate possible patterns of defect propagation. Conceivably, the formation energy distribution in a nonhomogeneously deforming CNT may indicate the possible weak spot where a defect is most likely to occur if the environment permits its nucleation.

Many researchers have addressed the problem of computing the formation energy of the SW defects in carbon nanotubes, as well as in boron-nitride tubes. Some papers focused on quantifying the change of chemical bond energy due to defect reconfiguration [Zhang et al. 1998; Zhang and Crespi 2000; Pan et al. 2000; Zhou and Shi 2003; Bettinger et al. 2002; Dumitrica et al. 2003; Piquini et al. 2005]. Typically, for this purpose, small isolated patches of atoms were considered. Nevertheless, the formation energy includes the contribution from elastic distortion. Strictly speaking, the energy variation should be considered at the structural level. At present, various levels of theories from *ab initio* calculations to molecular dynamics (MD) simulations have been applied to structural energetics computation. The MD approach as in [Moon and Hwang 2004a; 2004b; Marques et al. 2005] can handle relatively large systems. It should be noted that different theories do lead to different predictions [Grossman et al. 1995; Bettinger et al. 2002].

In this paper, we present a method for computing the structural energetic variation of SW transformation in pre-loaded CNTs. The method rests on the observation that a 5-7-7-5 ring is a local defect, in the sense that the elastic distortion is confined to a local region and diminishes rapidly after a short distance. If long range interactions such as the Coulomb force can be neglected, the energetic variation would result primarily from defective bond reconfiguration and the local elastic distortion. In Section 2, a formula for the relative Gibbs free energy is derived, in which the relative energy is expressed as a sum of the change of potential in the local defective region and an elastic correction that approximates the influences of the remaining system. The formula suggests an efficient way to compute the formation energy in relatively large scale atomic systems. Instead of computing the global energetics of the defective system, one only considers an embedded local defective cluster, and takes into account the remaining system through the correction term. The reduction allows one to readily perform structural level energetic analysis. For example, one can employ the method to compute the formation energy map, that is, the formation energy distribution in nonhomogeneously deforming systems. Likewise, one can study the energetic interaction between multiple defects by placing new defects in a pre-defective system. With the proposed method, global configuration optimization is performed only once. This local scheme works for classical potentials with finite range interaction. In Section 4, the method is applied to carbon nanotubes where the bond energy is modeled by the Brenner potential [Brenner 1990].

2. Structural formation energy of Stone–Wales defect

We consider CNTs at low temperatures where the thermal fluctuation is negligibly small and the atomic system remains approximately in a quasiequilibrium state. The formation of a defect causes a change of the total energy in the system. The difference

$$E_f = \Pi^{(2)} - \Pi^{(1)} \tag{1}$$

defines the formation energy, where $\Pi^{(1)}$ and $\Pi^{(2)}$ are the Gibbs free energies of the reference and the defective systems. As alluded to earlier, the energy difference should primarily result from the reconfiguration of sp^2 bonds in the defect and its distortion to the surrounding lattices. Inspired by Eshelby's method for the inclusion problem [Eshelby 1957] and his approach to defect energetics [Eshelby 1975], we propose a local approach for computing the energy difference of the entire system.

Figure 2 illustrates the notions used in the localization method. The local cluster D is a small set of atoms in which a 5-7-7-5 dislocation is to be embedded. The set of atoms that is the complement of D in the pristine domain is denoted by P. The interface set, denoted by I, includes the atoms in D that have energetic interaction with any atom in P and vice versa. For pairwise interaction, the interface set contains the bonding pairs along the internal boundary. For many-body potentials the interface may extend to a thin layer of atoms. We employ the Brenner bond order potential [1990] to model the bond energy. The interface set consists of the atoms on the layer of hexagon rings directly connecting D and P (see Figure 2). In addition, we identify the atoms in P that are subject to external load as the boundary set B, which can be further divided into disjoint subsets $B = B_r \cup B_t$ corresponding to displacement and force boundary points.

Consider a reference tube subject to the load

$$\begin{aligned} \mathbf{r}_i^{(1)} &= \bar{\mathbf{r}}_i, &\qquad \text{for atom } i \in B_r,\\ \mathbf{t}_i^{(1)} &= \bar{\mathbf{t}}_i, &\qquad \text{for atom } i \in B_t. \end{aligned}$$

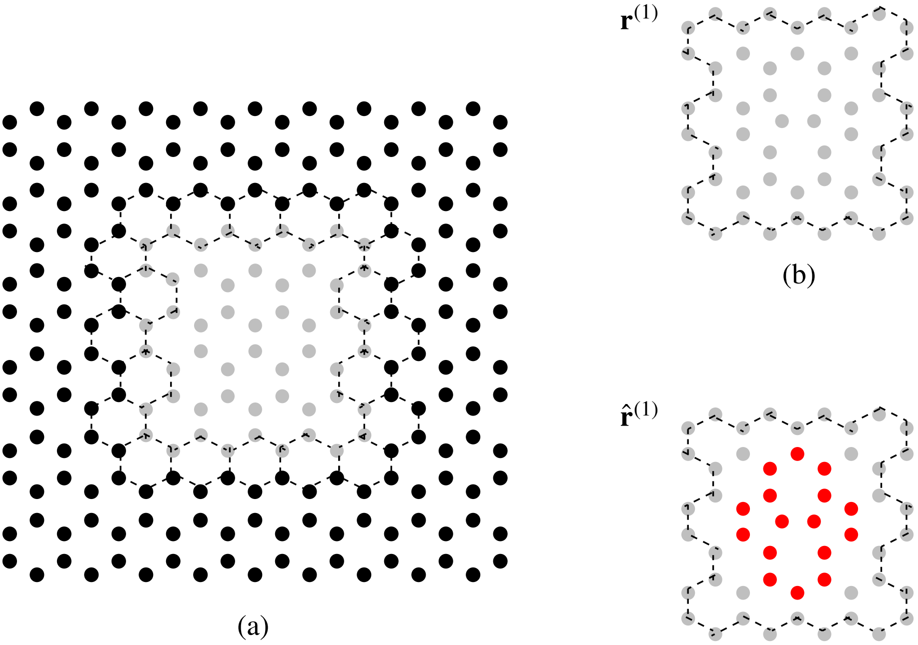

(a)

(b)

(c)

Figure 2. Schematics of the method. (a) Gray dots represent the atoms of the local cluster D and black dots represent pristine atoms. The interface is marked by the layer of dashed hexagon rings; (b) The deformed local region with the atom positioned at $\mathbf{r}^{(1)}$; (c) The defective replica $\widehat{D}$, whose boundary is fixed, but interior atoms are allowed to relax.

Let $\mathbf{r}_j^{(1)}$ be the coordinates of atom j at equilibrium. Under the same external load, a defective tube with a SW dipole embedded in D produces a different equilibrium state $\mathbf{r}^{(2)}$. The Gibbs free energies of the reference and the defective tubes are

$$\begin{aligned}\Pi^{(1)} &= E_{P+D}(\mathbf{r}^{(1)}) - \sum_{b\in B_t} \bar{\mathbf{t}}_b \cdot \mathbf{r}_b^{(1)},\\ \Pi^{(2)} &= E_{P+\widehat{D}}(\mathbf{r}^{(2)}) - \sum_{b\in B_t} \bar{\mathbf{t}}_b \cdot \mathbf{r}_b^{(2)}.\end{aligned} \tag{2}$$

The total interatomic potential consists of the sum of bond energies V_{ij} and can be regrouped into the sum of site potentials E_i. We write

$$E_{P+D} = \sum_{i<j} V_{ij} = \sum_{i\in P+D} E_i. \tag{3}$$

With Brenner potential and the threefold bond structure, the energy of site i is

$$E_i = \frac{1}{2}\sum_j V_{ij}, \tag{4}$$

where the sum runs over the three sp^2 bonds connecting to atom i. The potential of the whole tube can be naturally split into $E_{P+D} = E_P + E_D$, where each term consists of the sum of site energies in the respective region.

For the succeeding development, we introduce an auxiliary configuration $\hat{\mathbf{r}}^{(1)}$ of the defective tube using an imaginary fixing and replacing process: (1) Select a region D into which a 5-7-7-5 ring is to be inserted; (2) Fix all the interface atoms; (3) Replace the interior atoms in D with a defective replica. The interior atoms in D do not directly interact with the interior atoms in P and hence, once the interface atoms are constrained, any reconfiguration in D will not induce atomic displacements in P. However, a set of force (called mismatch force) is needed on the interface atoms to keep the them from moving. This imaginary process leads to a configuration

$$\hat{\mathbf{r}}_i^{(1)} = \begin{cases} \mathbf{r}_i^{(1)} & \text{if } i \in P \cup I, \\ \hat{\mathbf{r}}_i^{(1)} & \text{if } i \in \widehat{D} \setminus I. \end{cases}$$

Imagine that one isolates the local cluster D and keeps it in the deformed state $\mathbf{r}^{(1)}$. To sustain the deformation, one must apply a set of forces, denoted by $\mathbf{t}^{(1)}$, on the interface atoms. This set of forces corresponds the internal force that interface atoms experience in the reference state $\mathbf{r}^{(1)}$. Likewise, to deform the defective replica $\widehat{D}$ to the auxiliary configuration, one must apply another set of forces $\hat{\mathbf{t}}^{(1)}$ on the interface atoms. By equilibrium, the difference $\hat{\mathbf{t}}^{(1)} - \mathbf{t}^{(1)}$ is the interface mismatch force that is necessary to sustain the configuration $\hat{\mathbf{r}}^{(1)}$ in addition to the original boundary forces that are left intact.

We now return to the computation of formation energy. The difference in free energy between the auxiliary and the reference structure is

$$E_{\widehat{D}}(\hat{\mathbf{r}}^{(1)}) - E_D(\mathbf{r}^{(1)}). \tag{5}$$

If the mismatch force is gradually released, the defective tube will relax to the final defective configuration $\mathbf{r}^{(2)}$. If the tube is subject to all displacement boundary conditions, the work done by gradually releasing the mismatch force can be approximated as

$$-\frac{1}{2} \sum_{s,t \in I} (\hat{\mathbf{t}}_s^{(1)} - \mathbf{t}_s^{(1)}) \cdot \mathbb{C}_{st} (\hat{\mathbf{t}}_t^{(1)} - \mathbf{t}_t^{(1)}). \tag{6}$$

where $\mathbb{C}_{st}$ is the compliance matrix associated with the interface atoms evaluated at the auxiliary configuration. Since the relaxation process is elastic, the work reflects the change of potential from the auxiliary to the final configuration. Adding (5) and (6), the change of free energy from the reference to the final defective state can be approximated as

$$E_f \approx E_{\widehat{D}}(\hat{\mathbf{r}}^{(1)}) - E_D(\mathbf{r}^{(1)}) - \frac{1}{2} \sum_{s,t \in I} (\hat{\mathbf{t}}_s^{(1)} - \mathbf{t}_s^{(1)}) \cdot \mathbb{C}_{st} (\hat{\mathbf{t}}_t^{(1)} - \mathbf{t}_t^{(1)}). \tag{7}$$

In the Appendix, we show that the same formula applies to the force boundary condition as well. Thus, the formula furnishes a unified local scheme for the computation of the formation energy. The leading term $E_{\widehat{D}}(\hat{\mathbf{r}}^{(1)}) - E_D(\mathbf{r}^{(1)})$ gives a first order approximation to the structural energy variation. The remaining term represents structural influence. If the mismatch force is small, this term provides a second order correction to the formation energy.

Our experience indicates that the compliance matrix can be replaced by the corresponding compliance of the reference tube without causing a noticeable difference in the formation energy. This leads to further simplification in the computation, since the compliance matrix of the reference system can be readily obtained during configuration optimization.

3. Computational procedure

The molecular mechanics (MM) method with the implementation proposed in [Liu et al. 2004a] is employed to obtain the equilibrium state of the CNT under loads. The MM calculation is based on the energy minimization with respect to discrete atomic positions. The free energy in the system is

$$\Pi = E(\mathbf{r}) - \sum_{k \in B_t} \bar{\mathbf{t}}_k \cdot \mathbf{r}_k \tag{8}$$

The first generation Brenner potential [1990; 1992] is used to model CNT bond energy. The parameters listed as potential I in [Brenner 1990] are used in the computation.

The equilibrium of the atomic system requires that atomic positions cause the total potential energy to reach its minimum

$$\frac{\partial \Pi}{\partial \mathbf{r}_i} = 0, \tag{9}$$

subjected to $\mathbf{r}_i = \bar{\mathbf{r}}$ on B_r. This yields a nonlinear system of $3(N - N_{B_r})$ equations where N is the total number of atoms and N_{B_r} the number of atoms subject to boundary displacements. To find equilibrium atomic positions, the Newton–Raphson method is employed to solve the equations of (9). At the k-th iteration (configuration), the increments of the atomic coordinates are given by

$$\left[\frac{\partial^2 \Pi}{\partial \mathbf{d} \partial \mathbf{d}}\right]\Bigg|_{\mathbf{d}^{(k)}} \Delta \mathbf{d}^{(k+1)} = -\frac{\partial \Pi}{\partial \mathbf{d}}\bigg|_{\mathbf{d}^{(k)}}, \tag{10}$$

where

$$\mathbb{K} := \frac{\partial^2 \Pi}{\partial \mathbf{d} \partial \mathbf{d}}$$

is the tangent stiffness matrix (the Hessian), and $\mathbf{d}$ is the vector of atomic displacements. The system (10) is solved iteratively until convergence is achieved.

At convergence we partition the stiffness matrix $\mathbb{K}$ into

$$\mathbb{K} = \begin{bmatrix} \mathbb{K}_{ss} & \mathbb{K}_{sd} \\ \mathbb{K}_{ds} & \mathbb{K}_{dd} \end{bmatrix}, \tag{11}$$

where s stands for the degrees of freedom of the interface atoms I, and d denotes the remaining degrees of freedom. The compliance matrix $\mathbb{C}$ in (7) is computed according to

$$\mathbb{C} = (\mathbb{K}_{ss} - \mathbb{K}_{sd} \mathbb{K}_{dd}^{-1} \mathbb{K}_{sd})^{-1}.$$

The procedure for computing the energy difference is summarized as follows:

1. Compute the equilibrium configuration of the reference tube.
2. At the position where a SW ring is to be inserted, select a local cluster, identify the interface, and record the coordinates of the interface atoms.

3. Replace the cluster with a defective replica, solve a local equilibrium problem to compute the atomic coordinates in the replica keeping interface atoms fixed from step 2.
4. Compute the relative energy according to Equation (7).

Global configuration optimization is performed only once, on the reference tube. This reduction allows one to efficiently compute the defect energetics in a relatively large system, and also to compute the relative energy as the defect position varies. If the structure has unconstrained rigid body modes (typical in MD simulations), the tangent stiffness $\mathbb{K}$ is singular and hence the compliance cannot be directly computed. In this case, one can eliminate the rigid body singularity by augmenting $\mathbb{K}$ with several rank-one updates $\sum_{\alpha} a_{\alpha}\mathbf{R}_{\alpha} \otimes \mathbf{R}_{\alpha}$, where α ($\alpha \leq 6$) is the number of rigid body modes, $\mathbf{R}_{\alpha}$ are the modes vectors, $\mathbb{K}\mathbf{R}_{\alpha} = \mathbf{0}$, and a_{α} are positive scalars. This will not affect the energy computation since the matching force $\hat{\mathbf{t}}^{(1)} - \mathbf{t}^{(1)}$ is self-equilibrium. The proof of this fact is straightforward.

4. Results and discussion

Cluster size. The proposed method is based on the premise that if the size of the local cluster is sufficiently large, the mismatch force should be small, so Equation (7) should provide a second-order accurate estimation for the formation energy. For practical purposes, it is of foremost importance to investigate the influence of cluster size on the energy computation. We used two types of clusters. For large diameter tubes we introduced the layer patch as shown in Figures 1(a) and (b). The pentagon-heptagon ring itself (bold solid line), which has 16 atoms, is defined as the layer-0 patch. The region enclosed by dashed lines, with 42 atoms, is termed layer-1; the layer-2 region is enveloped by the dotted line. These types of clusters are consistent with the defect-shell model of [Zhou and Shi 2003]. For small diameter tubes, the ring model was introduced. A defective ring is a tube segment that contains a SW defect. Figure 1(c) shows the family of hierarchically defined defective rings in a (5,5) armchair tube. The ring-1 corresponds to the segment that just contains a 5-7-7-5 dipole, the ring-2 extends to two additional layers of atoms, and so on. The corresponding ring models in a (10,0) zigzag appear in Figure 1(d). Note that a 5-7-7-5 dipole has three possible orientations in each chirality [Zhou and Shi 2003]. Here we consider the one in which the pentagon-pentagon axis points predominantly along the tube axis.

We considered tubes under axial tension by prescribed end-displacement. A SW defect is inserted in a 5 nm long (10,10) armchair and a 5 nm long (17,0) zigzag. Figures 3(a) and 3(b) show the values of formation energy obtained using clusters of various sizes. It is seen that, for the (10,10) armchair, the local cluster as small as layer-0 can yield results almost identical to those by the full tube. The high accuracy may be attributed to the relatively minor distortion the SW defect produces in the armchair configuration. In contrast, Figure 3(b) shows that the layer-2 cluster is necessary to achieve a comparable accuracy in the (17,0) zigzag owing to the relatively large distortion the SW defect produces in a zigzag tube.

The analyses were repeated for the 12 nm long (5,5) armchair and the (10,0) zigzag shown in Figure 4 using the defective ring. Figures 3(a) and 3(b) present the formation energy results. For the armchair, the ring-1 and the ring-2 results are almost identical and both are very close to the full tube result. On the contrary, for zigzag tube the ring-1 results show a moderately large deviation from the full tube result. The ring-2 cluster seems necessary for an accurate estimation. The formation energies of the SW defect are found to approach zero when the strain is around 6% for armchair tubes and around 12% in zigzag tubes. These values agree nicely with existing reports [Buongiorno Nardelli et al. 1998a].

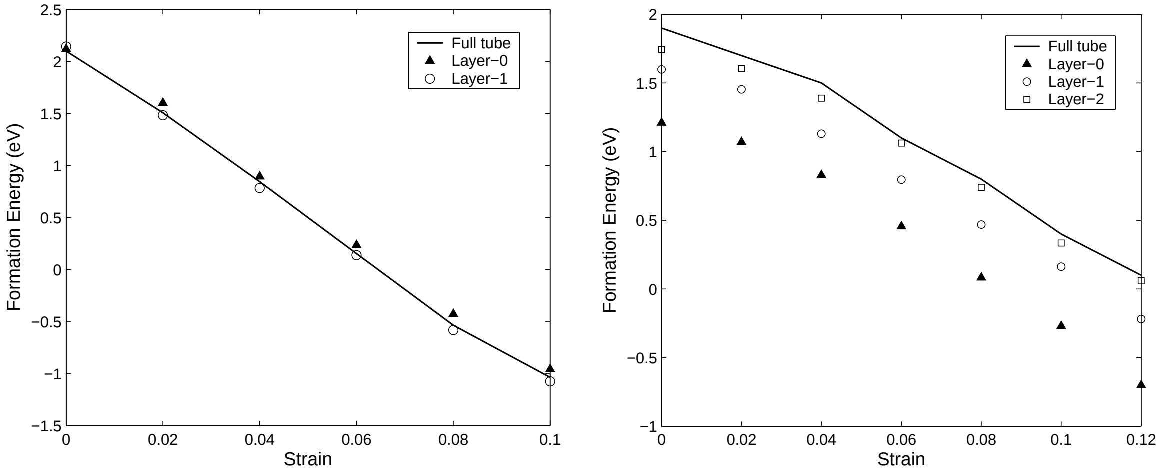

(a) armchair (10,10)

(b) zigzag (17,0)

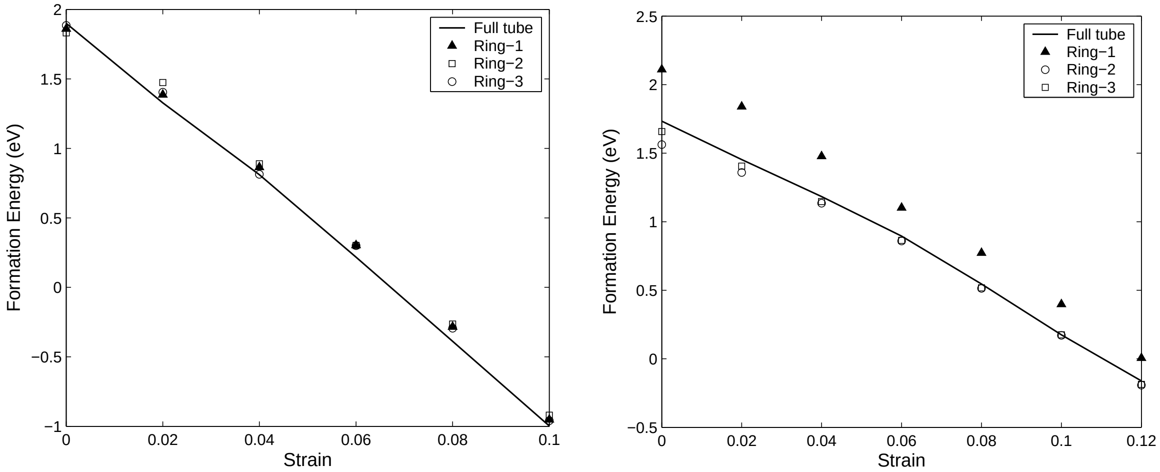

(c) armchair (5,5)

(d) zigzag (10,0)

Figure 3. Comparative formation energies versus stretch.

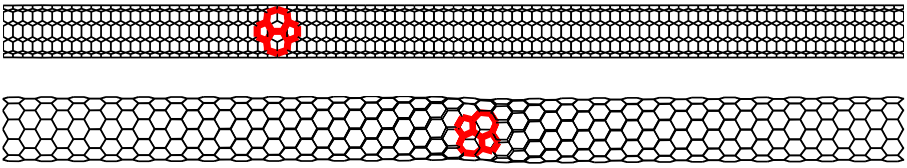

Figure 4. Slender tubes (12nm) used in the computation. Top: (5,5) armchair. Bottom: (10,0) zigzag.

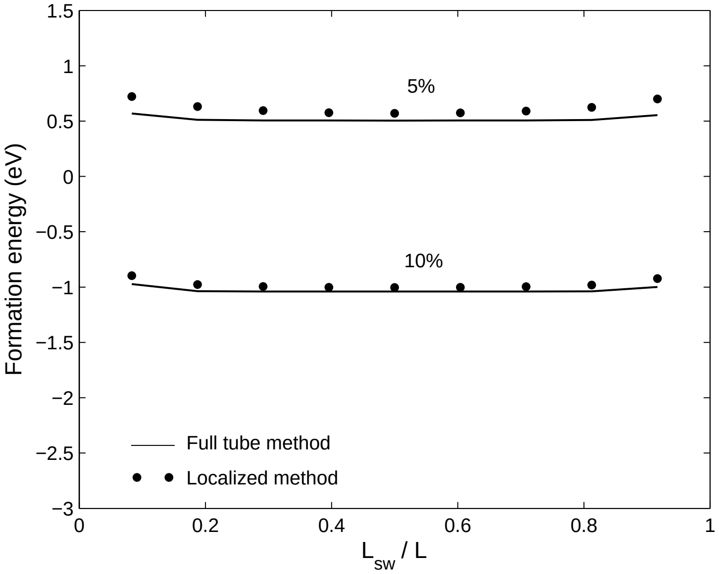

Figure 5. Distribution of formation energy in the uniformly stretched nanotube.

Formation energy map. In a nonuniformly deforming CNT, the defect formation energy depends on the local strain (stress) level and factors such as the distance to the tube boundary. Hence, the spatial distribution of formation energy provides an indicator for the potential weak spot where a defect transformation is most likely to occur. We applied the method to study the formation energy distribution. We first considered a 12 nm long (5,5) armchair under axial tension. Nine locations uniformly placed along the tube length were chosen where a SW dipole was to be inserted. The formation energies were calculated for these nine locations respectively, assuming a single SW defect appears in the tube for each time. The ring-1 model was employed; see Figure 1(c). Figure 5 presents the formation energy distribution under three levels of strain.

Notably, the formation energy possesses a symmetric distribution and attains its lowest value in the middle, implying that the defect transformation is most likely to initiate near the middle. Although the reference state is uniform, the formation energy shows a small variation across the tube length due to boundary effects. For a further assessment of accuracy, the full tube results are also computed. The approximate results agree well with the full tube computations in most locations, except near the ends of the tube, where the solutions deviate slightly.

Bending is a common mode of deformation that slender CNTs are likely to experience. We calculated the formation energies of the 12nm (5,5) armchair in four bent configurations shown in Figure 6. Configurations (a) and (b) were obtained by applying a transverse force at the tip; and configurations (c) and (d) were obtained by prescribing end-displacement. Since we were interested in stretch-induced SW rotation, the defect was inserted in the stretched side of the tube. The same nine locations were employed. In configurations (a) and (b), the maximum bending moment occurs at the fixed end while in (c) and (d) the maximum bending occurs in the middle of the tube. Figure 7 shows the formation energy distribution. For (a) and (b), where maximum bending appears at the end, the lowest formation

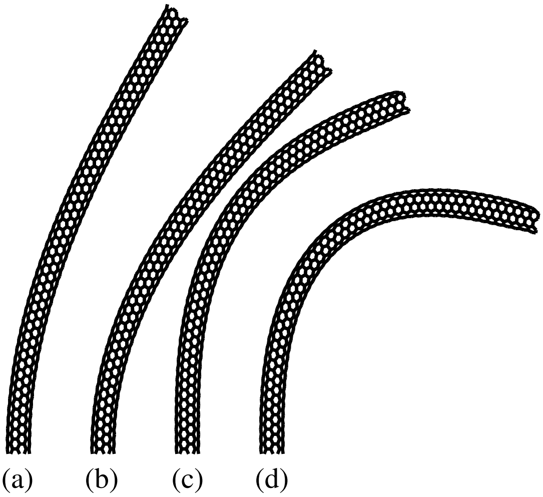

Figure 6. Four bent configurations of the (5,5) carbon nanotube.

energy is found near the end. In contrast, for (c) and (d), formation energy is lowest in the middle. The distribution indicates that the formation energy correlates directly with the bending moment, which is expected since the latter determines the local stretch in the tube. Figure 7 also includes the results from full tube computation. The approximate results are found to be close to the full tube solution in most locations. Only near the boundary does the solution show minor deviations.

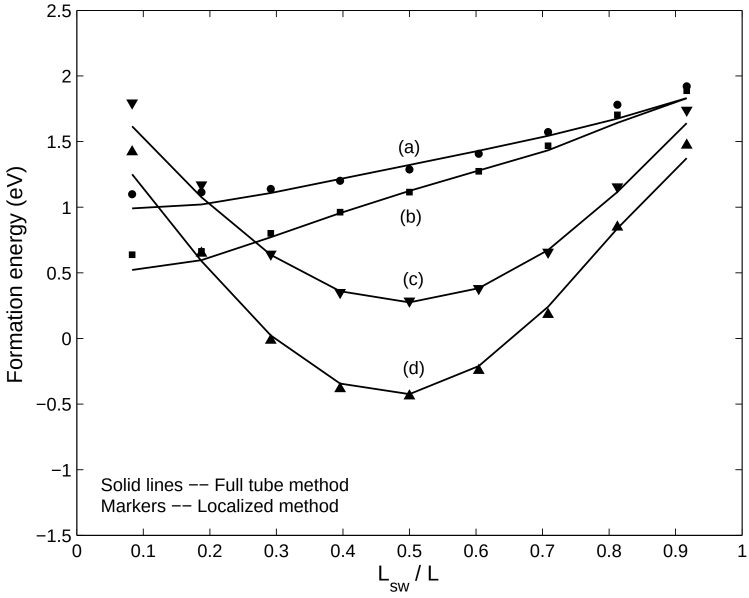

Figure 7. The distribution of formation energy on bent (5,5) nanotubes. Curves (a) through (d) correspond to the configurations in Figure 6.

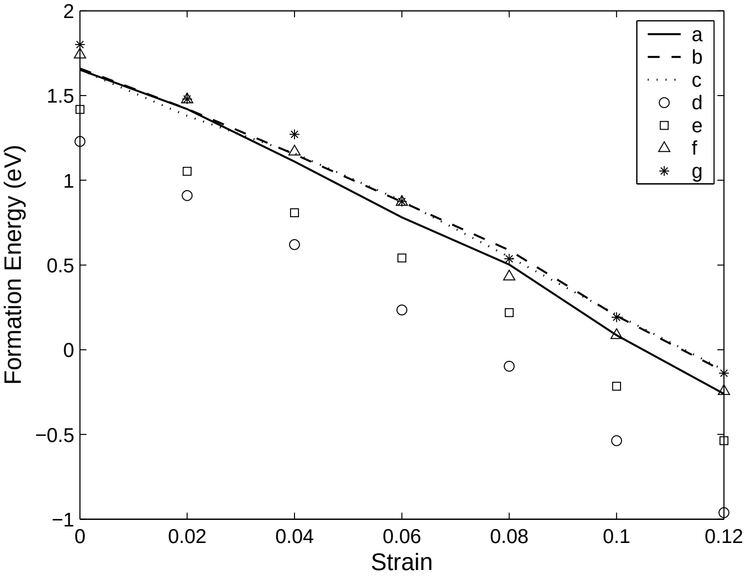

Figure 8. Interaction energy between two defects. The cases (a) through (f) correspond to the relative positions illustrated in Figure 9.

Defect interaction. Samsonidze et al. [2002a] reported that when two SW defects are placed close to each other, the formation energy varies with their relative position and orientation, indicating that two defects may repulse or attract each other depending on their relative position. We studied the interaction of SW defects in stretched tubes using the proposed method. Figure 9 shows a defective (10,0) tube having a primary SW defect and a secondary defect inserted at various positions. We considered the following cases: axially adjacent (a); axially distanced (b) and (c); diagonally adjacent (d); axially skewed (e); and diagonally distanced (f) and (g). For locations (b) and (c), we employed the ring-1 model for each defect. A larger ring enclosing two SW defects (see part (e) of Figure 9) was used for other cases. The interaction is characterized by the difference of the Gibbs free energies with and without the second defect.

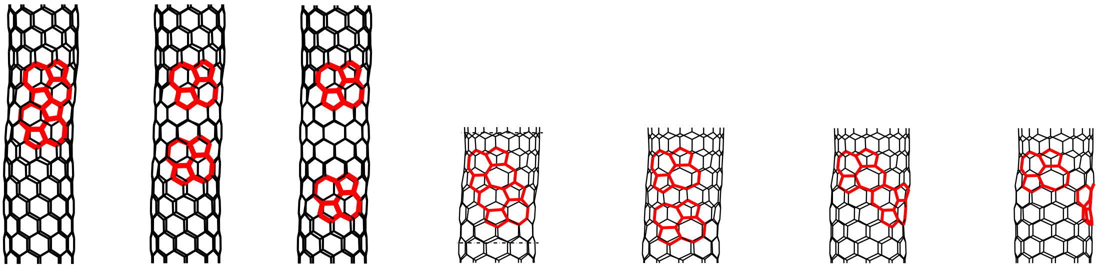

(a) (b) (c) (d) (e) (f) (g)

Figure 9. Relatively positioned multiple defects.

The energy curves are presented in Figure 8. The diagonally adjacent case (d) shows the lowest interaction energy across the strain range, indicating that such a configuration is most favorable. The axially skewed location (e) has the second lowest energy across the strain range. Although the defects are closely packed in (a), the energy is only slightly lower than other cases where the defects are further separated, suggesting that axially adjacent defects are less likely to appear in a zigzag tube. It is seen that if the defects are sufficiently distanced from each other, the interaction energies appear to be insensitive to the relative position. While the pattern of orientation dependence appears to agree with the early report in [Samsonidze et al. 2002a], the lack of interaction for distanced defects may be a consequence of the Brenner potential which vanishes after a short cut-off distance.

5. Summary

We have proposed a method to compute the structural energetic variation induced by the formation of a SW defect. The method exploits the local nature of a SW defect and yet properly takes into account the energetic influence from the remaining system. The advantage lies in the computational efficiency in comparison to other methods routinely used in computation of formation energy. Within the framework of MD (or MM) computation, the method provides an efficient way to study SW energetics at the structural level. The method applies to systems where the interaction is of finite range. In such systems the influence of bond reconfiguration can be localized. If long range interactions, such as the Coulomb force, are significant, the nonlocal effect needs to be carefully considered.

Appendix: Derivation of Equation (7)

Starting from Equations (1) and (2), adding and subtracting the boundary term $\sum_{s\in I}\mathbf{t}_s^{(1)}\cdot(\mathbf{r}_s^{(2)}-\mathbf{r}_s^{(1)})$ gives

$$\begin{aligned} E_f \equiv \Pi^{(2)}-\Pi^{(1)} = \Big(& E_P(\mathbf{r}^{(2)}) - E_P(\mathbf{r}^{(1)}) - \sum_{b\in B_t}\bar{\mathbf{t}}_b\cdot(\mathbf{r}_b^{(2)}-\mathbf{r}_b^{(1)}) - \sum_{s\in I}(-\mathbf{t}_s^{(1)})\cdot(\mathbf{r}_s^{(2)}-\mathbf{r}_s^{(1)})\Big) \\ &+\Big(E_{\widehat{D}}(\mathbf{r}^{(2)}) - E_D(\mathbf{r}^{(1)}) - \sum_{s\in I}\mathbf{t}_s^{(1)}\cdot(\mathbf{r}_s^{(2)}-\mathbf{r}_s^{(1)})\Big), \end{aligned} \tag{12}$$

where $\mathbf{t}_s^{(1)}$ is the internal force exerted on the interface atoms to maintain D in the reference state $\mathbf{r}^{(1)}$. Adding and subtracting terms further, the energy difference can be written as

$$\begin{aligned} E_f = \Big(& E_P(\mathbf{r}^{(2)}) - E_P(\mathbf{r}^{(1)}) - \sum_{b\in B_t}\bar{\mathbf{t}}_b\cdot(\mathbf{r}_b^{(2)}-\mathbf{r}_b^{(1)}) - \sum_{s\in I}(-\mathbf{t}_s^{(1)})\cdot(\mathbf{r}_s^{(2)}-\mathbf{r}_s^{(1)})\Big) \\ &+\Big(E_{\widehat{D}}(\mathbf{r}^{(2)}) - E_{\widehat{D}}(\hat{\mathbf{r}}^{(1)}) - \sum_{s\in I}\hat{\mathbf{t}}_s^{(1)}\cdot(\mathbf{r}_s^{(2)}-\mathbf{r}_s^{(1)})\Big) \\ &+ E_{\widehat{D}}(\hat{\mathbf{r}}^{(1)}) - E_D(\mathbf{r}^{(1)}) + \sum_{s\in I}(\hat{\mathbf{t}}_s^{(1)}-\mathbf{t}_s^{(1)})\cdot(\mathbf{r}_s^{(2)}-\mathbf{r}_s^{(1)}). \end{aligned} \tag{13}$$

In what follows the two terms in large parentheses will be simplified. The first term corresponds to the energy variation in region P under the variation of atomic positions $\mathbf{r}^{(1)} \to \mathbf{r}^{(2)}$. By Taylor expansion,

$$E_P(\mathbf{r}^{(2)}) - E_P(\mathbf{r}^{(1)}) = \sum_{i\in P} \left.\frac{\partial E}{\partial \mathbf{r}_i}\right|_{\mathbf{r}^{(1)}} \cdot \Delta\mathbf{r}_i + \frac{1}{2}\sum_{i,j\in P} \Delta\mathbf{r}_i \cdot \left[\left.\frac{\partial^2 E}{\partial \mathbf{r}_i \partial \mathbf{r}_j}\right|_{\mathbf{r}^{(1)}} \Delta\mathbf{r}_i \right] + \mathrm{O}(|\Delta\mathbf{r}|^3)\ , \tag{14}$$

where $\Delta\mathbf{r}_i = \mathbf{r}_i^{(2)} - \mathbf{r}_i^{(1)}$. Invoking the virtual work principle, we have

$$\sum_{i\in P} \left.\frac{\partial E}{\partial \mathbf{r}_i}\right|_{\mathbf{r}^{(1)}} \cdot \Delta\mathbf{r}_i = \sum_{b\in B_t} \bar{\mathbf{t}}_b \cdot \Delta\mathbf{r}_b + \sum_{s\in I} (-\mathbf{t}_s^{(1)}) \cdot \Delta\mathbf{r}_s \tag{15}$$

Substituting (15) and (14) into the first bracket in (13), we find that the first order terms vanish, leaving

$$\frac{1}{2}\sum_{i,j\in P} \Delta\mathbf{r}_i \cdot \left[\left.\frac{\partial^2 E}{\partial \mathbf{r}_i \partial \mathbf{r}_j}\right|_{\mathbf{r}^{(1)}} \Delta\mathbf{r}_j \right] + \mathrm{O}(|\Delta\mathbf{r}|^3). \tag{16}$$

The domain sum term can be converted into boundary sum. With repeated use of the virtual work principle we can deduce

$$\sum_{i\in P} \Delta\mathbf{r}_i \cdot \left[\left.\frac{\partial^2 E}{\partial \mathbf{r}_i \partial \mathbf{r}_j}\right|_{\mathbf{r}^{(1)}} \Delta\mathbf{r}_j \right] = -\sum_{s\in I} (\mathbf{t}_s^{(2)} - \mathbf{t}_s^{(1)}) \cdot (\mathbf{r}_s^{(2)} - \mathbf{r}_s^{(1)}) + \mathrm{O}(|\Delta\mathbf{r}|^3)\ . \tag{17}$$

Combining (16) and (17), the expression inside the first bracket in (13) reduces to

$$-\frac{1}{2}\sum_{s\in I} (\mathbf{t}_s^{(2)} - \mathbf{t}_s^{(1)}) \cdot (\mathbf{r}_s^{(2)} - \mathbf{r}_s^{(1)}) + \mathrm{O}(|\Delta\mathbf{r}|^3)\ . \tag{18}$$

Applying the same procedure to the second bracket yields

$$E_{\widehat{D}}(\mathbf{r}^{(2)}) - E_{\widehat{D}}(\hat{\mathbf{r}}^{(1)}) - \sum_{s\in I} \hat{\mathbf{t}}_s^{(1)} \cdot (\mathbf{r}_s^{(2)} - \hat{\mathbf{r}}^{(1)}) = \frac{1}{2}\sum_{s\in I} (\mathbf{t}_s^{(2)} - \hat{\mathbf{t}}_s^{(1)}) \cdot (\mathbf{r}_s^{(2)} - \mathbf{r}_s^{(1)}) + \mathrm{O}(|\Delta\mathbf{r}|^3). \tag{19}$$

Substituting (18) and (19) into (13), we conclude

$$E_f = E_{\widehat{D}}(\hat{\mathbf{r}}^{(1)}) - E_D(\mathbf{r}^{(1)}) + \frac{1}{2}\sum_{s\in I} (\hat{\mathbf{t}}_s^{(1)} - \mathbf{t}_s^{(1)}) \cdot (\mathbf{r}_s^{(2)} - \mathbf{r}_s^{(1)}) + \mathrm{O}(|\Delta\mathbf{r}|^3), \tag{20}$$

where $\hat{\mathbf{t}}_s^{(1)} - \mathbf{t}_s^{(1)}$ is the mismatch force. The final position $\mathbf{r}^{(2)}$ can be obtained by relaxing the mismatch force, or equivalently by applying a set of equal and opposite forces on the interface. To the first order, the interface atoms incremental displacements induced by the relaxation can be computed by

$$\mathbf{r}_s^{(2)} - \mathbf{r}_s^{(1)} = -\sum_{s,t\in I} \mathbb{C}_{st}(\hat{\mathbf{t}}_t^{(1)} - \mathbf{t}_t^{(1)}), \tag{21}$$

where $\mathbb{C}$ is the current compliance associated with the interface atoms. In light of this, we can further write

$$E_f = E_{\widehat{D}}(\hat{\mathbf{r}}^{(1)}) - E_D(\mathbf{r}^{(1)}) - \frac{1}{2}\sum_{s,t\in I} (\hat{\mathbf{t}}_s^{(1)} - \mathbf{t}_s^{(1)}) \cdot \mathbb{C}_{st}(\hat{\mathbf{t}}_t^{(1)} - \mathbf{t}_t^{(1)}) + \mathrm{O}(|\Delta\mathbf{r}|^3). \tag{22}$$

It is evident that Equation (7) is second-order accurate with respect to the magnitude of the mismatch force. If the potential energy is quadratic, the formula becomes exact.

References

[Bettinger et al. 2002] H. F. Bettinger, T. Dumitrică, G. E. Scuseria, and B. I. Yakobson, "Mechanically induced defects and strength of BN nanotubes", *Phys. Rev. B* **65**:4 (2002), 041406.

[Brenner 1990] D. W. Brenner, "Empirical potential for hydrocarbons for use in simulating the chemical vapor deposition of diamond films", *Phys. Rev. B* **42**:15 (1990), 9458–9471.

[Brenner 1992] D. W. Brenner, "Erratum: Empirical potential for hydrocarbons for use in simulating the chemical vapor deposition of diamond films", *Phys. Rev. B* **46**:3 (1992), 1948–1948.

[Buongiorno Nardelli et al. 1998a] M. Buongiorno Nardelli, B. I. Yakobson, and J. Bernholc, "Mechanism of strain release in carbon nanotubes", *Phys. Rev. B* **57**:8 (1998), R4277–R4280.

[Buongiorno Nardelli et al. 1998b] M. Buongiorno Nardelli, B. I. Yakobson, and J. Bernholc, "Brittle and ductile behavior in carbon nanotubes", *Phys. Rev. Lett.* **81**:21 (1998), 4656–4659.

[Chandra et al. 2004] N. Chandra, S. Namilae, and C. Shet, "Local elastic properties of carbon nanotubes in the presence of Stone–Wales defects", *Phys. Rev. B* **69**:9 (2004), 094101.

[Choi et al. 2000] H. J. Choi, J. Ihm, S. G. Louie, and M. L. Cohen, "Defects, quasibound states, and quantum conductance in metallic carbon nanotubes", *Phys. Rev. Lett.* **84**:13 (2000), 2917–2920.

[Dumitrica et al. 2003] T. Dumitrica, H. F. Bettinger, G. E. Scuseria, and B. I. Yakobson, "Thermodynamics of yield in boron nitride nanotubes", *Phys. Rev. B* **68**:8 (2003), 085412.

[Eshelby 1957] J. D. Eshelby, "The determination of the elastic field of an ellipsoidal inclusion, and related problems", *Proc. R. Soc. Lond. A* **241**:1226 (1957), 376–396.

[Eshelby 1975] J. D. Eshelby, "The elastic energy-momentum tensor", *J. Elasticity* **5**:3–4 (1975), 321–335.

[Grossman et al. 1995] J. D. Grossman, L. Mitas, and K. Raghavachari, "Structure and stability of molecular carbon: importance of electron correlation", *Phys. Rev. Lett.* **75**:21 (1995), 3870–3873.

[Liu et al. 2004a] B. Liu, Y. Huang, H. Jiang, S. Qu, and K. C. Hwang, "The atomic-scale finite element method", *Comput. Methods Appl. Mech. Eng.* **193**:17–20 (2004), 1849–1864.

[Liu et al. 2004b] B. Liu, H. Jiang, H. T. Johnson, and Y. Huang, "The influence of mechanical deformation on the electrical properties of single wall-carbon nanotubes", *J. Mech. Phys. Solids* **52**:1 (2004), 1–26.

[Marques et al. 2005] L. A. Marques, L. Pelaz, M. Aboy, P. Lopez, and J. Barbolla, "A novel technique for the structural and energetic characterization of lattice defects in the molecular dynamics framework", *Comput. Mater. Sci.* **33**:1–3 (2005), 112–117.

[Mielke et al. 2004] S. L. Mielke, D. Troya, S. L. Zhang, J. L. Li, S. Xiao, R. Car, R. S. Ruoff, G. C. Schatz, and T. Belytschko, "The role of vacancy defects and holes in the fracture of carbon nanotubes", *Chem. Phys. Lett.* **390**:4–6 (2004), 413–420.

[Moon and Hwang 2004a] W. H. Moon and H. J. Hwang, "A force field approach of structure and formation energy of defects of boron nitride nanotubes with tetragon-octagon pairs", *Mater. Lett.* **58**:17–18 (2004), 2331–2334.

[Moon and Hwang 2004b] W. H. Moon and H. J. Hwang, "Molecular-dynamics simulation of defect formation energy in boron nitride nanotubes", *Phys. Lett. A* **320**:5 (2004), 446–451.

[Nordlund and Hakonen 2005] K. Nordlund and P. Hakonen, "Nanotube: controlling conductance", *Nat. Mater.* **4**:7 (2005), 514–515.

[Pan et al. 2000] B. C. Pan, W. S. Yang, and J. Yang, "Formation energies of topological defects in carbon nanotubes", *Phys. Rev. B* **62**:19 (2000), 12652–12655.

[Piquini et al. 2005] P. Piquini, R. J. Baierle, T. M. Schmidt, and A. Fazzio, "Formation energy of native defects in BN nanotubes: an ab initio study", *Nanotechnology* **16**:6 (2005), 827–831.

[Samsonidze et al. 2002a] G. G. Samsonidze, G. G. Samsonidze, and B. I. Yakobson, "Energetics of Stone–Wales defects in deformations of monoatomic hexagonal layers", *Comput. Mater. Sci.* **23**:1–4 (2002), 62–72.

[Samsonidze et al. 2002b] G. G. Samsonidze, G. G. Samsonidze, and B. I. Yakobson, "Kinetic theory of symmetry-dependent strength in carbon nanotubes", *Phys. Rev. Lett.* **88**:6 (2002), 065501.

[Stone and Wales 1986] A. J. Stone and D. J. Wales, "Theoretical studies of icosahedral C_{60} and some related species", *Chem. Phys. Lett.* **128**:5–6 (1986), 501–503.

[Troya et al. 2003] D. Troya, S. L. Mielke, and G. C. Schatz, "Carbon nanotube fracture: differences between quantum mechanical mechanisms and those of empirical potentials", *Chem. Phys. Lett.* **382**:1–2 (2003), 133–141.

[Yakobson 1998] B. I. Yakobson, "Mechanical relaxation and intramolecular plasticity in carbon nanotubes", *Appl. Phys. Lett.* **72**:8 (1998), 918–920.

[Zhang and Crespi 2000] P. Zhang and V. H. Crespi, "Plastic deformations of boron-nitride nanotubes: an unexpected weakness", *Phys. Rev. B* **62**:16 (2000), 11050–11053.

[Zhang et al. 1998] P. Zhang, P. E. Lammert, and V. H. Crespi, "Plastic deformations of carbon nanotubes", *Phys. Rev. Lett.* **81**:24 (1998), 5346–5349.

[Zhao et al. 2002] Q. Zhao, M. Buongiorno Nardelli, and J. Bernholc, "Ultimate strength of carbon nanotubes: a theoretical study", *Phys. Rev. B* **65**:14 (2002), 144105.

[Zhou and Shi 2003] L. G. Zhou and S.-Q. Shi, "Formation energy of Stone–Wales defects in carbon nanotubes", *Appl. Phys. Lett.* **83**:6 (2003), 1222–1224.

Received 27 Feb 2006. Accepted 27 Jun 2006.

LIANG ZHANG: `lianzhan@engineering.uiowa.edu`
Department of Mechanical and Industrial Engineering, Center for Computer Aided Design, The University of Iowa,
Iowa City, IA 52242-1527, United States

JIA LU: `jia-lu@uiowa.edu`
Department of Mechanical and Industrial Engineering, Center for Computer Aided Design, The University of Iowa,
Iowa City, IA 52242-1527, United States